Applied Catalysis B: Environmental 217 (2017) 365–377

Contents lists available at ScienceDirect

Applied Catalysis B: Environmental

journal homepage: www.elsevier.com/locate/apcatb

V_2O_5-WO_3/TiO_2 catalysts under thermal stress: Responses of structure and catalytic behavior in the selective catalytic reduction of NO by NH_3

Patrick G.W.A. Kompio[a,1], Angelika Brückner[b], Frank Hipler[c], Olga Manoylova[d], Gerhard Auer[c,2], Gerhard Mestl[d], Wolfgang Grünert[a,*]

[a] Lehrstuhl Technische Chemie, Ruhr-Universität Bochum, D-44801 Bochum, Germany
[b] Leibniz-Institut für Katalyse e. V. (LIKAT) Rostock, D-18059 Germany
[c] Huntsman P & A Germany, D-47198 Duisburg, Germany
[d] Clariant Produkte (Deutschland) GmbH, Werk Heufeld, D-83052 Bruckmühl, Germany

ARTICLE INFO

Article history:
Received 22 March 2017
Received in revised form 31 May 2017
Accepted 3 June 2017
Available online 6 June 2017

Keywords:
NH_3-SCR
V_2O_5-WO_3/TiO_2 catalysts
Thermal activation
Thermal deactivation
Promoter influence

ABSTRACT

V_2O_5-WO_3/TiO_2 catalysts of compositions typically used in SCR applications were subjected to calcinations in air at temperatures between 873 K and 1023 K for different durations, starting from a mildly calcined state in which species structure originating from wet preparation had been fixed by calcination at 623 K for 1 h. After calcination, samples were examined with respect to their SCR activity and to structural changes by nitrogen physisorption, XRD, Raman spectroscopy, EPR, temperature-programmed reduction, XPS and Low-Energy Ion Scattering (LEIS). Driven by loss of BET surface area, samples exhibited a complex behavior with up to three well-separated maxima of SCR activity before final deactivation. While the first of these maxima depended on the calcination rate (temperature), the other two maxima occurred at specific ranges of the BET surface area. During calcination, tungstate was segregated from the support surface forming WO_3 under more severe conditions. Observations in the EPR spectra are in conflict with assignments of observed SCR activities to isolated vanadate sites. Assuming major contributions of dimeric vanadate to the catalytic performance, a model was proposed, which explains the first two activity maxima while the origin of the third one remains to be elucidated. In this model, segregation of tungstate results in formation of active V-O-V structures from less active isolated vanadate species previously separated by excessive amounts of tungstate. The main role of tungstate is to provide optimum sizes of vanadate ensembles, but a direct favorable influence of tungstate on vanadate is not excluded.

1. Introduction

Selective catalytic reduction of nitrogen oxides by ammonia (NH_3-SCR) is a traditional approach to the removal of harmful nitrogen oxides (NO_x) from stationary emission sources [1]. Meanwhile it has been developed into the key step of present technology for NO_x abatement in the exhaust of Diesel and lean gasoline engines (urea-SCR [2]). The ammonia reductant reduces NO_x selectively to nitrogen (e.g., for NO):

$$2\,NO + 4\,NH_3 + O_2 \rightarrow 4\,N_2 + 6\,H_2O$$

In urea-SCR of passenger Diesel vehicles, the NO_x reduction step of urea-SCR is usually catalyzed by redox zeolites. Technology for stationary sources remains to be dominated by catalysts that contain V_2O_5 and WO_3 supported on TiO_2 (anatase). They are meanwhile also applied for mobile sources, in particular in heavy utility vehicles, where they are adapted to the different targets [1,2]. Therefore, scientific interest in these catalysts remains at high level despite their long history. In typical formulations for stationary sources, the active vanadium component is kept below 2 wt-% [3,4], while 10 wt-% is a typical content of the WO_3 promoter [1,4,5]. The promoter is described to increase activity, widen the tempera-

* Corresponding author at: Lehrstuhl Technische Chemie, Ruhr-Universität Bochum, Universitätsstraße 150, D-44801 Bochum, Germany.
E-mail address: w.gruenert@techem.ruhr-uni-bochum.de (W. Grünert).
[1] Present address: IAV GmbH, D-38518 Gifhorn, Germany.
[2] Present address: Xtract GmbH, D-78462 Konstanz, Germany.

http://dx.doi.org/10.1016/j.apcatb.2017.06.006
0926-3373/

ture range in which catalysts are selective to N_2 formation, and to stabilize their physical surface area [3–8].

All discussions are based on widely accepted knowledge that interactions between the TiO_2 support and V(V) or W(VI) oxide species result in surface oxide phases structurally very different from the bulk oxides [9–11] and changing with the surface coverage. In dehydrated V_2O_5/TiO_2 catalysts, the structures range from isolated distorted tetrahedral V oxide species (a short V=O bond above three V-O-Ti bridges to the support) via two-dimensional oligomeric/polymeric metavanadates to disordered, and finally crystalline V_2O_5 nanoparticles at high V content [9,10,12–16], While the surface oxide species do not grow into the third dimension in well-prepared catalysts before the support is completely covered by the 2d surface oxide phase [17,18], clusters and bare support surface may coexist in suboptimal preparations. In recent work, we observed, however, that there is a tendency of surface V oxide species in V_2O_5/TiO_2 catalysts to aggregate into 2-dimensional islands, which could be detected by EPR at coverages as low as 3% [19].

In dehydrated WO_3/TiO_2 catalysts, strongly distorted octahedral surface species ($(-O)_5$-W = O) were reported to predominate up to high tungsten oxide coverages [12]. In V_2O_5-WO_3/TiO_2 catalysts, they were found to coexist with isolated and polymeric surface vanadates. It was reported that the abundance of polymeric species increased with growing tungsten content at metal coverages considerably exceeding the monolayer limit if both metals are thought to compete for the same surface sites [12]. Recently, we found by EPR and temperature-programmed reduction studies that surface W oxide species disrupt surface V oxide islands which results in a well-mixed surface oxide phase characterized by close neighborhood between isolated V and W oxide species [19].

The debate on the nature of active sites has long been dominated by the view that SCR proceeds on dimeric (or oligomeric) surface V(V) oxo species [20–25]. While there is clear evidence that reaction rates per V ion increase significantly with the vanadium content [23,25], results at low V contents suggest an activity contribution also from isolated sites. Their intrinsic activity was estimated to be an order of magnitude lower than that of dimeric sites [23]. SCR activity of isolated sites has been proposed very early [26], and was clearly confirmed in zeolite-based catalysts [27,28], where the sites are, however, not stable under harsh conditions [28]. For isolated sites, a mechanism involving NH_3 activation via reduction by V(V) (nitrosamide mechanism) was proposed [29,30]. On the other hand, Brønsted sites (V-OH) were claimed to be involved in NH_3-SCR as well [31–33]. A catalytic cycle combining with the dimeric nature of the active sites, which was proposed by Topsøe et al. [34–37] on the basis of *in-situ* FT-IR and reaction studies, has been supported by many groups. Very recently, however, strong support for the nitrosamide route has been provided by Marberger et al. [38] on the basis of transient spectroscopic (IR, UV–vis) experiments with modulation excitation and phase-sensitive detection. These data obviously support a monomeric nature of the active site, but the authors did not comment on the earlier evidence on average turnover frequencies of vanadium sites increasing with vanadium content.

The reasons why tungsten promotes the active vanadium sites are still under debate. Relevant experimental evidence includes increased acidity in the presence of tungsten, which might favor ammonia supply for the reaction [6,39], an increased reducibility of the V component in presence of tungsten [6], which should be relevant for SCR being a redox reaction, and the delayed transformation from monomeric vanadyl to crystalline V_2O_5 during ageing [40], which excludes the latter as a source of activity. The stabilizing effect of tungsten oxide on the TiO_2 support [41,42], concerns stability rather than activity. The view that tungstates occupying a significant part of the support surface enforce a closer proximity on the surface V oxide species encouraging thus the formation of the most active V-O-V structures [6] has been challenged by our earlier results, which show that tungsten destroys rather than creates surface V oxide islands [19]. This does not yet explain the nature of the promotion, which might arise from the vicinity of a more acidic element (W) or from an electronic effect of the tungsten on the nearby vanadium site. A third choice should be included if the dimeric nature of the active sites is accepted: the activity of these sites might depend on the size of the islands containing them, e.g. if only the rims are active or if addition of a third V already interferes with the catalytic function.

Work presented in this paper follows the idea that the behavior of V_2O_5-WO_3/TiO_2 catalysts under thermal stress may provide further insight into the catalytic effects of W-O-V neighborhood, because the resulting reduction of the BET surface area may cause one of the components to predominantly segregate from the surface. Literature available on this topic and experience in industry suggest that there is no simple relation between thermal stress and deactivation. Indeed, Madia et al. found higher activities after treatment at higher temperatures in particular for catalysts with low V content [4], Nova et al. reported increased activity at decreased N_2 selectivity after calcination at 1073 K [43]. On the other hand, Beale et al. recently reported a monotonous loss of activity upon severe calcination, which was alleviated by doping the support with SiO_2 [44]. After subjecting catalysts of different composition to high-temperature treatments, Augustine et al. observed both slight activation and deactivation without obvious trends [45]. Kobayashi and Hagi [46] reported that the activity of a SiO_2-containing V_2O_5-WO_3/TiO_2 catalyst goes through a maximum upon calcination at 823 K. The observations were largely explained by increased amounts of more active polyvanadates due to competition between surface V and W oxide species for the decreasing support surface. We have now studied the effect of high-temperature treatments on this catalyst type in more detail by subjecting a typical sample to temperatures between 873 and 1023 K for different times and monitoring the effect of this treatment on activity, BET surface area, phase composition, reducibility of transition metal species, and site structure by various techniques including XRD, TPR, Raman and EPR spectroscopy, XPS, and Low-energy Ion Sputtering (LEIS).

2. Experimental

2.1. Catalyst preparation and basic properties

Catalysts were prepared starting from a titania oxide hydrate in the anatase modification, for which an ignition loss of 11.9 %, a specific surface area of >250 m^2/g, a density of 3.8 g/cm^3, a sulfate content of <2%, and impurity contents of Fe_2O_3 and Na_2O <100 ppm each are specified by the manufacturer [47]. Sources of W and V were ammonium paratungstate ($(NH_4)_{10}(H_2W_{12}O_{42})\cdot 4H_2O$, APT, Tima Tungsten GmbH, impurity elements <0.0088 wt-%) and ammonium metavanadate (NH_4VO_3, Acros, 99%).

WO_3 was deposited on the TiO_2 hydrate by wet impregnation of APT from its aqueous solution, the concentration of which was chosen to obtain a WO_3 loading of 10.0 wt-%. The material was dried at 383 K overnight and calcined in flowing synthetic air (20% O_2/He) at 713 K for 1 h, which brought the BET surface area down to 142 m^2/g. This material was wet impregnated with an aqueous NH_4VO_3 solution to obtain a loading of 1.5 wt-% V_2O_5, followed by overnight drying at 383 K. The resulting catalyst with a W/V atomic ratio of 2.6, has been labelled $V_{1.5}W_{10}$. Transition metal coverages can be evaluated using known data for areal densities in the monolayer. Unfortunately, there is disagreement in literature regarding this important parameter: according to Ref. [48], one m^2 support surface can accommodate 12.7 μmol V or 6.8 μmol W, according to

Ref. [49] somewhat less (10.4 μmol V or 4.6 μmol W). In the following, we will report values calculated with the data of ref. 47. After the preparation of $V_{1.5}W_{10}$, which did not change the BET surface area significantly, the total transition metal ion coverage was 54%.

Two catalysts with different metal oxide contents were also prepared to investigate the influence of the catalyst composition on the effects of the high-temperature treatment. In one of them, the V_2O_5 content was decreased to 0.5 wt-% ($V_{0.5}W_{10}$, W/V = 7.8$_5$). With an initial BET surface area of 112 m^2/g, its initial transition metal coverage was 60%. The other catalyst was made with a WO_3/TiO_2 precursor precalcined at 790 K, and the WO_3 and V_2O_5 contents were 5.4 and 1.5 wt-% ($V_{1.5}W_{5.4}$, W/V = 1.4). With an initial BET surface area of 63 m^2/g, the transition metal coverage in this sample was 75% initially.

2.2. Thermal treatments and catalytic measurements

Different protocols for air calcination were applied to these catalysts as will be detailed in the results section. All calcinations of up to 84 h (≈5000 min) duration were performed in flowing synthetic air in the catalytic setup, longer calcinations were made in stagnant air in a muffle furnace. Activity data will be related to the activity obtained after a very mild standard calcination (1 h at 623 K), which was applied already in our previous study [19] and was meant to just fix the spontaneous speciation of surface V and W species obtained after the impregnation process.

Catalytic data were measured in a micro flow reactor (inner diameter – 4.2 mm) with a feed gas mixture containing 1000 ppm NO, 1000 ppm NH_3, and 2 % O_2 in He. Experiments were made with a modified residence time W/F of $3.3 * 10^{-3}$ g s ml^{-1} (catalyst mass – 10 mg, feed flow – 183.3 ml min^{-1}). With an approximate bed density of 0.68 g cm^{-3} deduced from the bed height obtained, this results in a GHSV of ≈750,000 h^{-1}. Measurements were made between 423 and 873 K, in 50 K intervals. The temperature was raised at 5 K min^{-1} and conversions were recorded after achieving steady state. NO and NH_3 conversions were routinely determined via non-dispersive IR photometry (NO: BINOS 1004®/NH_3: BINOS 1000®), using an empirical correction for a minor cross-sensitivity of the NH_3 channel for the reaction product water. A NO_2 analyzer included in the analytical scheme did not indicate significant NO_2 formation in these runs. Key experiments were repeated with an N_2O analyzer (URAS 26) included. In these experiments, N_2 balances could be closed typically within ±5%.

We are aware that our choice of using dry feed may raise concerns about the relevance of our data for practical situations due to the water content of real flue gases. We have studied the influence of moisture on the performance of $V_{1.5}W_{10}$, but also of $V_{0.5}W_{10}$, after standard calcination by switching between feeds of the above-mentioned composition without and with 5 vol-% H_2O [50]. In presence of water, NO conversion was moderately reduced, to an extent corresponding to a 20–35% loss of activity if assessed by first-order rate constants. On this basis we propose that the phenomena reported below would have been observed also in the presence of moisture, with other values of conversion though, but exhibiting the same tendencies, which are the essence of our results.

2.3. Catalyst characterization

The catalyst was characterized in various states by nitrogen physisorption, XRD, Raman spectroscopy, EPR, temperature-programmed reduction, XPS, and Low-energy Ion Scattering (LEIS). Specific surface areas were determined by nitrogen physisorption using a Quantachrome Autosorb-1 MP instrument. Prior to analysis, the samples were outgassed for 2 h at 573 K. Phase compositions of the catalyst in the initial state and after most severe treatments were characterized by XRD measurements in reflection geometry with an Empyrean Theta–Theta diffractometer (Panalytical, Almelo) using a Cu anode (λ = 1.54056 Å). The K-beta emission line was suppressed by a Ni Filter. Additional experiments aiming at a more detailed resolution of the calcination process were performed in an *in-situ* camera attached to a D8 Advance instrument (Bruker AXS), using CuKα radiation as well, at 40 kV and 40 mA. Temperature-programmed reduction was made with 4.5% H_2 in Ar, ramping the temperature to 1073 K or 1273 K at 10 K min^{-1}. The effluent gas was analyzed by a Hydros thermal conductivity detector (Fisher-Rosemount).

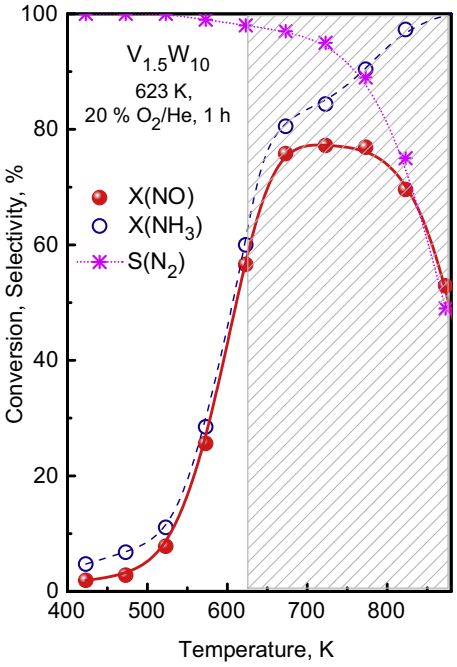

Fig. 1. NO and NH_3 conversions and nitrogen selectivities during the SCR of NO with ammonia over the standard V_2O_5-WO_3/TiO_2 catalyst ($V_{1.5}W_{10}$) calcined at 623 K for 1 h (reference state).
1000 ppm NO, 1000 ppm NH_3, and 2 % O_2 in He, GHSV = 750,000 h^{-1}.

Raman spectra were measured with both Laser excitation and a conventional near-IR source. Laser Raman spectra were measured with a Renishaw Raman spectrometer, which uses an Ar Laser (20 mW) at a wave length of 514 nm, with a spectrometer resolution of 2 cm^{-1}. FT-Raman spectra were recorded on a Thermo Nicolet Vectra Plus Instrument using a wavelength of 1064 nm at 370 mW (resolution – 4 cm^{-1}). Samples were dehydrated prior to the measurements (1 h at 623 K in Ar).

EPR spectra of dehydrated samples were recorded with an ELEXSYS 500-10/12 CW spectrometer (Bruker) using a microwave frequency of 9.5 GHz (X band), a power of 6.3 mW, a modulation frequency of 100 kHz, and a modulation amplitude of 0.5 mT. Spectra were recorded at 77 K. Spectral intensities were normalized on the sample mass, therefore, intensities are directly comparable although an integration was not performed.

X-ray photoelectron and Low-energy ion scattering spectra (LEIS) were measured on a Leybold LH10 spectrometer equipped with an EA 10/100 multi-channel detector (Specs). XPS was measured with Al Kα radiation (V 2p, O 1s, W 4f, Ti 2p, and C 1s), binding energies (B. E.) were referenced to the Ti $2p_{3/2}$ line at 457.8 eV. In LEIS, samples were exposed to 2000 eV He ions provided by an IQE 12/38 ion gun, analysis was made at a scattering angle of 145°. Data were treated with the CasaXPS software. For XPS, satellites were subtracted and peak intensities were evaluated over Shirley backgrounds, for LEIS, peaks were integrated over linear backgrounds.

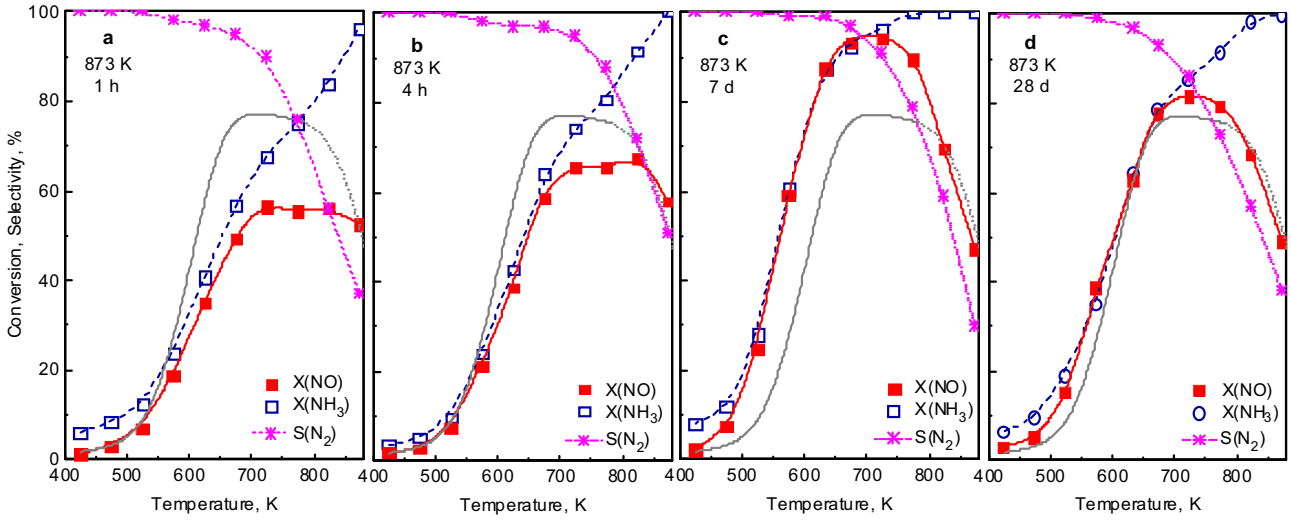

Fig. 2. NO and NH_3 conversions and nitrogen selectivities during the NH_3-SCR with $V_{1.5}W_{10}$ calcined at 873 K for different durations. For reaction conditions – see Fig. 1.

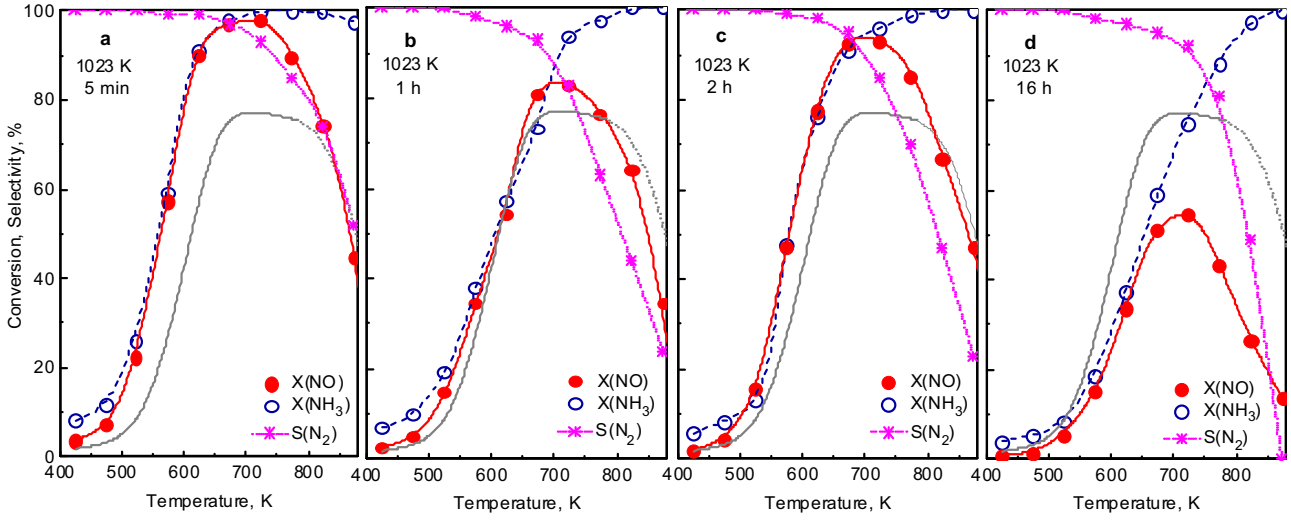

Fig. 3. NO and NH_3 conversions and nitrogen selectivities during the NH_3-SCR with $V_{1.5}W_{10}$ calcined at 1023 K for different durations. For reaction conditions – see Fig. 1.

3. Results and discussion

3.1. Catalytic behavior

Reactivity data of $V_{1.5}W_{10}$ in the reference state is shown in Fig. 1 where NO and NH_3 conversions and selectivity for N_2 are plotted *vs.* the reaction temperature. NO conversion has a broad maximum between 670 and 770 K ($X_{NO} \approx 78\%$). This is better than obtained with a similar catalyst reported in Ref. [19], where the preparation had, however, resulted in a somewhat lower BET surface area for unknown reasons. NH_3 conversions are virtually identical with NO conversions up to 623 K. Beyond this temperature, unselective NH_3 oxidation causes NH_3 conversion to further increase at constant NO conversion. NO formation by NH_3 oxidation is probably the reason behind the drop of NO conversion at the highest temperatures. N_2 selectivity is ≥95% up to 723 K. In Fig. 1, the temperature range above the original calcination temperature (623 K) has been hatched because the catalyst may suffer changes under these conditions. However, the conversion plateau starts quite near to the calcination temperature and is probably still characteristic of the surface obtained by fixation of the spontaneous arrangement of V and W during preparation. The NO conversion curve of Fig. 1 was included as a reference in all following conversion plots.

With this catalyst, calcination series have been performed at 873, 923, 973, and 1023 K, extended up to four weeks for the lowest temperature. In Figs. 2 and 3, examples for conversion curves measured after these calcinations are shown for treatments at 873 K and at 1023 K. According to Fig. 2a, an exposure to 873 K of just 1 h inflicted dramatic damage to the catalyst: plateau conversion decreased from 78% to 55%. However, the catalyst gradually recovered from this state, achieving 67% conversion already after 4 h and exceeding the initial state significantly after 7 days (≈10,000 min, X_{max} = 93%, Fig. 2b, c). Beyond, another decay of conversions suggests ultimate deactivation of the catalyst (Fig. 2d). The conversion curves resulting from calcination at 1023 K are even more spectacular. After a 5 min "shock treatment", the catalyst was strongly activated and achieved almost full conversion at 750,000 h^{-1} and a decrease of the light-off temperature T_{50} (temperature of 50% conversion) of almost 50 K relative to the reference state (Fig. 3a). After 1 h, peak NO conversion had already nearly returned to the initial value, but the decay of the curve beyond the maximum was steeper than initially (Fig. 3b). However, this decay was not the prelude of ultimate deactivation. Instead, a peak NO conversion beyond 90%

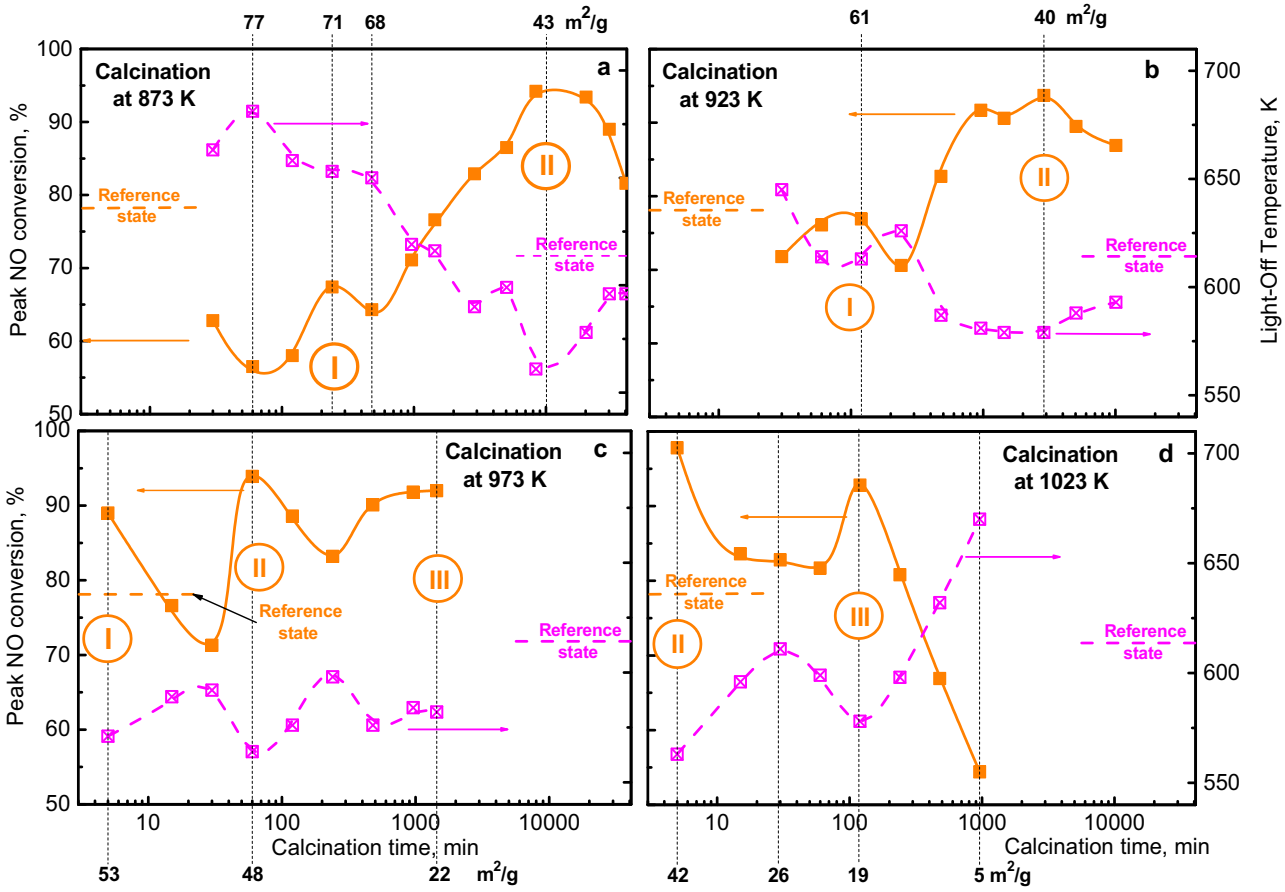

Fig. 4. Summary of calcination experiments. Peak NO conversions and light-off temperatures vs. duration of calcination at 873 K (a), 923 K (b), 973 K (c), and 1023 K (d), compared with peak NO conversion and light-off temperature in the reference state (calc. 1 h at 623 K; see marks at ordinates). BET surface areas of selected samples added at the abscissae. For reaction conditions – see Fig. 1.

was obtained after 2 h at 1023 K (Fig. 3c), and only beyond this time a deactivation was observed which seems to be irrevocable (Fig. 3d).

While drastically increased reaction rates could be observed after some of these thermal treatments, selectivity to nitrogen was generally deteriorated, although patterns were not straightforward. In the reference state (Fig. 1), N_2 selectivity fell below 90% beyond 760 K. This "T_{90}"decreased to 720 K after 1 h at 873 K, but achieved again almost 760 K after 2 h before it decreased to 730 K (7 d, ca. 10,000 min) and 605 K (28 d, ca. 40,000 min, Fig. 2). Already after 1 h at 1023 K, T_{90} was down to 680 K (5 min – 740 K), but it increased again to 695 K after 2 h and 730 K after 16 h. The latter increase is certainly due to a general deactivation of the catalyst. These trends, which apparently result from a complex superposition of changes in activation of NO and of NH_3 as well as of selectivity effects, will not be further commented.

In Fig. 4, information from activity tests after calcinations at the four temperatures mentioned above and for different durations are summarized by plotting peak NO conversions and light-off temperatures versus the calcination time, which is given on a logarithmic scale. The picture is rather unusual, with several NO conversion maxima and minima and corresponding minima and maxima of T_{50} following each other. At the lower calcination temperatures, short duration resulted in deterioration of the performance (Fig. 4a, b) while strong activation was obtained by short-time calcination at high temperature.

To examine the primary tendency caused by thermal stress, the same catalyst was also subjected to an extended calcination at only 623 K with samples taken after 1 and 2 weeks [51]. After 2 weeks, a BET surface area of 119 m^2/g was measured and peak NO conversion had decreased to ≈73%. This is hardly beyond experimental error, but as the whole conversion curves went consistently lower with increasing duration in this experiment, it is safe to conclude that the primary effect upon extending the mild reference calcination is deterioration. Therefore, the improvements seen at the start of the 973 K and 1023 K calcination series (Fig. 4c, d) appear beyond a minimum, which is not time-resolved at these high calcination temperatures. With this conversion minimum preceding the first point of the 973 K series (Fig. 4c), we have indeed three minima and three maxima before the catalyst finally dies off. The final decay has not been achieved in the 973 K series, but it is obvious in the 1023 K series (Fig. 4d). In the latter, the maximum after 2 h calcination corresponds to the third one of the 973 K series (at ≈1000 min). The first point after 5 min calcination at 1023 K corresponds to the second maximum at 973 K while the remaining features are not resolved. Under milder conditions (Fig. 4a, b), only the first and second maxima are covered, the third one may be expected after long weeks, with an intermediate deterioration of unknown extent in between.

It is instructive to compare catalytic data at the conversion maxima. The second one appeared in all series and afforded always NO conversions of almost 95% (at 1023 K even above). In these points of the calcination series, T_{50} was around 563 K, with the exception of the 923 K series where it remained at 578 K, and N_2 selectivity ranged between 91 and 94%. Peak NO conversions of >90% (at T_{50} of ≈573 K) were also observed at the third conversion maximum where it could be achieved (Fig. 4c, d). The first maximum was, however, rather variable: It was well pronounced only in the 973 K series (first point, $X_{NO,max}$ = 89%, T_{50} = 573 K), still doubtless

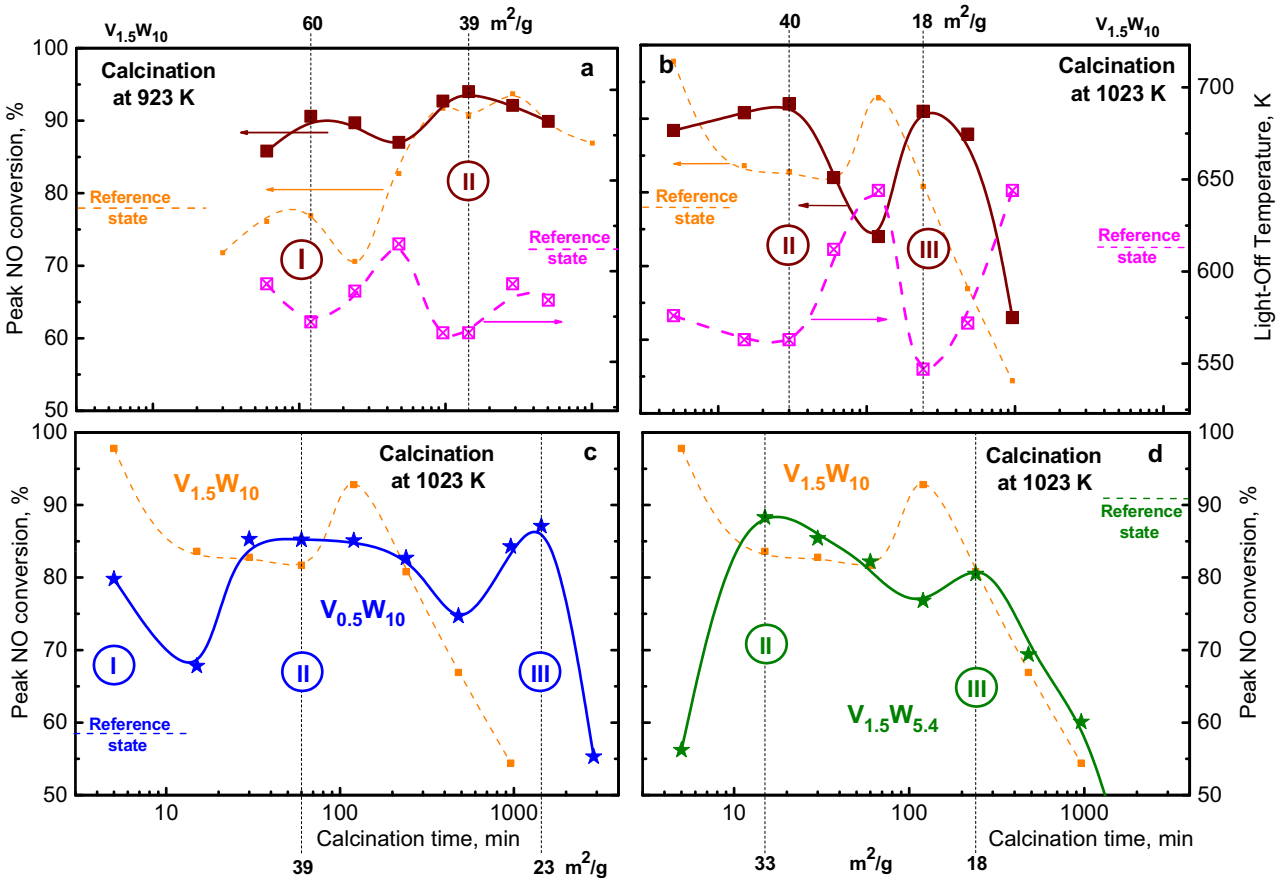

Fig. 5. Summary of calcination experiments under modified conditions. Peak NO conversions and light-off temperatures vs. duration of calcination at different temperatures, for general arrangement of figure – see Fig. 4. Calcination of $V_{1.5}W_{10}$ in moist air (10 vol-% H_2O) at 923 K (a) and at 1023 K (b), peak conversions in dry feed added in orange (small symbols) for comparison; calcination of $V_{0.5}W_{10}$ (c) and $V_{1.5}W_5$ (d) in dry air at 1023 K, only peak conversions; data of $V_{1.5}W_{10}$ added in orange for comparison. (For interpretation of the references to colour in this figure legend, the reader is referred to the web version of this article.)

at 923 K ($X_{NO,max}$ = 78%, T_{50} = 613 K), but hardly significant at 873 K ($X_{NO,max}$ = 68%, T_{50} = 653 K).

The structural parameter changing most obviously along the calcination series is the BET surface area, and data taken at selected points are added above and below the diagrams in Fig. 4. It can be observed that the surface area is rather characteristic for the second and the third maximum (≈20 m^2/g and ≈42 m^2/g, respectively, with an outlier at 973 K – 48 m^2/g). On the contrary, the BET surface area at the first maximum was less specific, decreasing from 71 m^2/g to 53 m^2/g with increasing calcination temperature, which is reminiscent of the variation in the peak conversions. Comparing the high definition of NO conversion and BET surface area for the 2nd and 3rd maxima with the variability of these properties in the first maximum, one may suppose that the former maxima are related to stable configurations of surface species, which are controlled mainly by the size of the support surface available, while the situation causing the first maximum seems to be influenced by the kinetics of ongoing solid-state processes. The situation achieved upon shock calcination at 973 K (Fig. 4c) appears to be metastable: when the system is allowed to develop more gradually, e.g. at lower temperatures (Fig. 4a, b), the situation characteristic for the 1st maximum tends to disappear.

As the BET surface area appears to be a crucial parameter with respect to the phenomena observed, the influence of moisture (10 vol-% H_2O) during the calcination procedure was examined as well, and the results for calcinations at 923 K and at 1023 K are depicted in Fig. 5a and b. The sequence of conversion peaks and minima mirroring the trends in the light-off temperature is much the same as for dry ageing, and the BET surface areas at which conversion peaks appear are unchanged. Unexpectedly, the time scale was expanded rather than contracted, which is very obvious by comparing dry and moist calcination at 1023 K (Fig. 5b) while the situation is less clear with the second maximum at 923 K (Fig. 5a). There was no significant influence of moisture during calcination on peak conversions in the second and third maxima, which were >90% in all cases, but the first maximum at 923 K was clearly affected: peak conversion increased from ≈78% to ≈90% (Fig. 5a). The delay of the conversion maxima on the time scale might be explained by considering that dehydroxylation of the titanium oxide hydrate is probably the driving force behind the loss of BET surface area. Such water desorption should be hindered in moist atmosphere.

Results obtained by calcination of catalysts of different compositions at 1023 K are summarized in Fig. 5c and d. The decrease of the vanadium oxide content (Fig. 5c) delayed the ageing process in accordance with earlier observations that supported WO_x species stabilize the surface area of TiO_2 [8,12], whereas supported VO_x species accelerate the shrinking process [41,52]. In this case, the reference state exhibited very low activity, and calcination resulted in notable improvements for almost all conditions applied. The opposite was observed for $V_{1.5}W_{5.4}$, which was highly active already in the reference state and suffered generally deterioration by the calcination process although conversion peaks and minima could be discerned here as well. Due to the small initial BET surface area (63 m^2/g), the surface state might be analogous to that in the first maximum in other samples, and the peaks obtained would correspond to the second and third maxima. Not unexpectedly, the

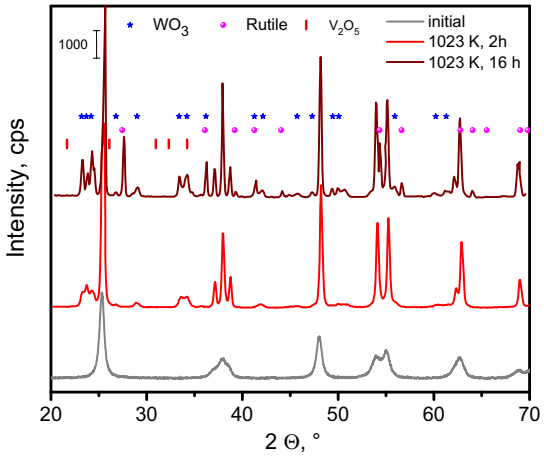

Fig. 6. XRD patterns of $V_{1.5}W_{10}$ after the reference calcination ("initial", 623 K, 1 h) and after 2 h and 10 h at 1023 K.

Table 1
Comparison of anatase particle sizes derived from XRD (Fig. 6) and from external surface areas.

Treatment	BET surface area, m^2/g	d_{BET}, nm[a]	d_{XRD} nm
reference (623 K, 1 h)	142	11	14.3
1023 K, 2 h	19	83	34
1023 K, 16 h[b]	5	315	42

[a] $d = \frac{6}{\rho S_{BET}}$, with ρ (density) of titania hydrate – 3.8 g cm^{-3} [47].
[b] 960 min.

BET surface areas at conversion peaks, which are also indicated in the figure, differ somewhat from those obtained with the $V_{1.5}W_{10}$ standard sample though falling still into the same ranges.

3.2. Structural characterization of $V_{1.5}W_{10}$ after calcination treatments

3.2.1. XRD

In Fig. 6, X-ray diffractograms of $V_{1.5}W_{10}$ in the reference state and after 2 h and 16 h (960 min) calcination at 1023 K are depicted. Diffractograms taken after other calcination treatments in an *in-situ* camera are reported in Fig. S1 in the Electronic Supplementary Information. Particle sizes of the dominating anatase phase, which have been derived from the data in Fig. 6 by the Scherrer equation using the line width of the (100) reflection at 2Θ = 25.43°, are given in Table 1. The decrease of these line widths with increasing calcination temperature (Fig. 6, S1) indicates the growth of the anatase coherence region. After 2 h at 1023 K, weak broad signals of WO_3 appeared together with the anatase lines (Fig. 6). After 16 h at this temperature they had grown narrower and more intense, and reflections of rutile became visible as well. Similar trends can also be seen in Fig. S1. However, in this series, the signals of segregated WO_3 were much more pronounced already after 2 h at 1023 K: apparently, conditions were more serious in the furnace than in the catalytic setup where treatments for the samples shown in Fig. 6 were performed. Inhomogeneity of temperature field in the furnace may be a reason for this. Nevertheless, no rutile was formed in this experiment, and neither WO_3 nor rutile were observed after 5 min at 1023 K and after 4 h at 873 K (Fig. S1). As the conditions were apparently more severe in the furnace than in the catalytic setup used for most calcination treatments preceding the catalytic runs (see above), rutile and WO_3 were obviously absent also in the corresponding samples used for catalysis. In no case, segregation of V_2O_5 or formation of a crystalline V-containing phase could be detected even after 16 h at 1023 K which reduced the BET surface area to 5 m^2/g. The observations on segregation of WO_3 and missing crystalline V-containing phases agree with results reported in ref. [44].

In Table 1, the particle sizes evaluated by XRD are compared with sizes derived from the BET surface area assuming spherical particle shape. While the values measured in the reference state are in good agreement, values diverge strongly and increasingly with more severe calcination: sizes derived from the external surface areas are larger than the XRD coherence regions. We presume that this arises from formation of polycrystalline aggregates at high temperatures, where particles may have been baked together occluding part of their surface phases and oxide crystallites segregated from them while excluding them from access by the gas phase.

3.2.2. Raman spectra

Laser Raman spectra (excitation wave length λ_{exc} = 514 nm) of these samples are displayed in Fig. 7. For 1 h calcination at 623 K (reference state) and 16 h (960 min) calcination at 1023 K, FT Raman spectra (λ_{exc} = 1064 nm) have been added for comparison after adapting the intensity scale. All spectra are dominated by the intense signals of anatase at 638, 515, 395, and 150 cm^{-1} (E_{1g}, A_{1g}/B_{1g}, B_{1g}, Eg modes; the E_g signal at 197 cm^{-1} was not resolved in most cases), which have been described in literature earlier [53,54]. The almost complete absence of signals from surface V or W species in the reference state has been reported already in ref. [19]. It was tentatively explained there by heterogeneities of the still strongly hydroxylated surface, which may cause structural inhomogeneity of the surface tungstate/vanadate species resulting in a distribution of their vibrational frequencies and disappearance of the expected signals [55].

These appeared already after 1 h calcination at 873 K (Fig. 7a) where a broad feature can be observed between 1050 and 780 cm^{-1}, which comprises a signal at 1020 cm^{-1} together with unresolved signals extending down to ca. 800 cm^{-1}. After 4 h at this temperature, the 1020 cm^{-1} signal and adjacent (unresolved) features were clearly increased. Upon further calcination at 873 K, intensity below 1000 cm^{-1} (at ca. 980 cm^{-1}) grew at the expense of the 1020 cm^{-1} signal, and the region around 800 cm^{-1} was enhanced and developed a well-defined peak at 808 cm^{-1}. At the same time, there was a change in the intensity ratio between anatase signals: the E_g signals grew relatively to the remaining ones (Fig. 7). This was most pronounced for the 638 cm^{-1} signal, but happened to a smaller extent also with the 150 cm^{-1} signal, which is, however, difficult to record correctly because of the nearby cutoff. While this agrees with observations made in ref. [44], our catalyst seems to be somewhat more stable than samples described in that paper. The spectrum after 5 min at 1023 K (Fig. 7b) is similar to the one after 1 h at 873 K (Fig. 7a). After 2 h at this temperature, the 1020 cm^{-1} signal had almost completely disappeared, the 808 cm^{-1} signal was well defined, and the just described intensity redistribution among the anatase bands occurred. Surprisingly, intensity above 780 cm^{-1} decreased again after 16 h calcination at 1023 K, which affects in particular the 808 cm^{-1} signal. This holds, however, only for the laser Raman spectrum: In the FT-Raman spectrum, this signal is very pronounced while the signals in the 900–1050 cm^{-1} range are completely missing.

In the 780–1050 cm^{-1} range, signals of terminal V = O and W = O bonds in isolated and oligomeric surface oxide species are expected [11–17,56,57]. The coexistence of signals from two elements complicates the assignment considerably [57,58]. Although the Raman cross section of surface V oxide species has been reported to be almost fourfold that of surface tungstate species [12,56], the latter will certainly contribute to the spectra due to the ca. 2.6 fold excess of W over V. On the other hand, Raman cross sections of bulk oxides, e.g. V_2O_5 are known to be much larger than those of surface

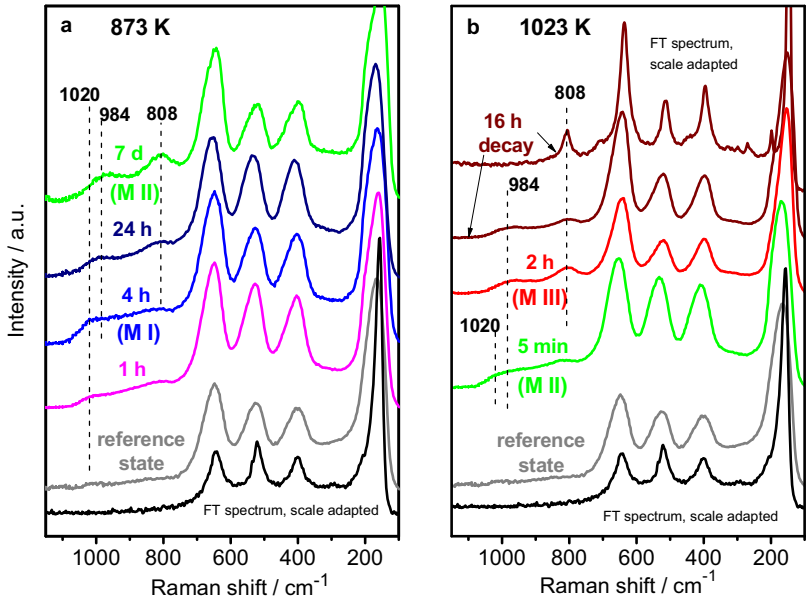

Fig. 7. Laser Raman spectra of $V_{1.5}W_{10}$ after the reference calcination (623 K, 1 h) and after different times at 873 K (a) or 1023 K (b); for comparison, selected FT Raman spectra are added, in (a) – spectrum of reference state, in (b) spectrum after 16 h at 1023 K. MI, MIII, MIII – 1st, 2nd, 3rd activity maximum.

oxide species [12,17,56,59–61]. Therefore, segregated oxides can be detected with good sensitivity.

The signal at 1020 cm^{-1} in Fig. 7a may arise from isolated surface vanadate sites while its extension to lower wave numbers may originate from oligomeric surface vanadates or from surface tungstate species. We believe that the enhanced intensity around 1000 cm^{-1} after 4 h at 873 K is still due to improved homogeneity of speciation while the transition of intensity from 1020 towards 980 cm^{-1} after 24 h at 873 K indicates the formation of oligomers and/or the segregation of surface species. The segregated phase is WO_3 (808 cm^{-1}). There is not any indication for segregation of V_2O_5, which would cause a sharp signal at 994 cm^{-1} [12]. The calcination series at 1023 K begins similar as the one at 873 K, but already after 2 h the 1020 cm^{-1} signal has almost disappeared and WO_3 can be clearly discerned. The decrease of intensity in the 1020–780 cm^{-1} region after 16 h at 1023 K can be assigned to the occlusion of surface species in polycrystalline aggregates (cf. Section 3.2.1). The presence of subsurface WO_3 is nicely demonstrated by the FT-Raman spectrum shown in Fig. 7. Because of smaller absorption at larger wavelength of the excitation radiation, this measurement is less surface sensitive [62] and correspondingly does not show the bands around 1000 cm^{-1} while the band of WO_3 is very intense. It should be noted that the assignments of transformations among surface oxide species have to remain tentative, but the predominant – and indeed exclusive – segregation of WO_3 from the surface during thermally induced decrease of the BET surface area is a well-supported result of the Raman study.

3.2.3. EPR spectroscopy

EPR spectra of $V_{1.5}W_{10}$ after thermal treatments are depicted in Fig. 8. Similar to the spectra of V_2O_5-(10% WO_3)/TiO_2 catalysts with varying V_2O_5 contents shown earlier [19] they consist of signals of isolated V(IV) species with hyperfine structure (hfs) superimposed on a broad isotropic background signal of magnetically interacting V(IV) sites within V_xO_y clusters formed by partial reduction of V(V) oxide species. Due to the absence of three-dimensional V_2O_5 structures indicated by the Raman spectra (section 3.2.2.) the isotropic signal can be ascribed to surface V oxide islands. During calcination at 873 K (Fig. 8a), the signal intensities of both the islands and the isolated species first increased significantly, but beyond 1 h, they exhibited a complex tendency. Direct comparison of the spectra suggests that both types of signals are decreased after 4 h (first maximum) and again increased after 8 h. After 7 days (≈10,000 h), both types of signals were clearly decreased. Calcination at 1023 K results in an obvious growth of the clustered phase, the signal of which was very intense after 16 h (960 min, Fig. 8b). After a strong increase relative to the reference state, the intensity of signals from isolated V(IV) species decreased on the whole, however, with an obvious intermediate increase in the activity minimum at 1 h.

Unfortunately, we were not able to substantiate these observations by quantitative modeling of the EPR spectra as had been successfully achieved with previous samples subjected to the reference calcination [19]. At the first glance, the spectra in Fig. 8 look rather similar to those analyzed previously except for intensity changes of the isotropic signal. However, although two different isolated V(IV) sites were superimposed with the isotropic background signal, many details could not be properly reproduced by spectra fitting. A simple comparison shows, however, that the EPR spectra do not convey direct information about the active sites of NH_3-SCR: the spectra after 1 h at 873 K (Fig. 8a) and after 5 min at 1023 K (Fig. 8b) are almost completely identical, but peak NO conversion was <60% in the former state (Fig. 2) and >95% in the latter state (Fig. 3). There is obviously no correlation between the abundance of any of the isolated sites detected and the development of activity with increasing treatment severity. On the other hand, the nature of the clustered phase is not unambiguously reflected by the isotropic EPR signal, since subtle alterations in the mutual magnetic interactions of V(IV) species within the clusters (caused by changes of the cluster size and/or shape) can alter the width of the isotropic signal significantly. Thus, the active sites may still constitute a subgroup of the clustered phase the signal of which cannot be singled out from the experimental EPR spectrum.

3.2.4. Temperature-programmed reduction

In Fig. 9, TPR profiles of $V_{1.5}W_{10}$ after different calcination treatments are compared with that obtained after reference calcination (Fig. 9a). The assignment of the signals has been derived in ref. [19] by comparison with W-free and V-free reference samples. On this basis, the peak around 770 K arises from simultaneous reduction of V(V) to V(III) and of W(VI) sites in the vicinity of V sites to W(IV)

while the signal at 870 K is caused by W(VI) species which are isolated or interacting with other tungstate groups. Reduction of W(IV) to W(0) happens above 1100 K. In all experiments, further hydrogen consumption was observed above 1200 K, which may arise from reduction of surface Ti^{4+} sites.

The most obvious trend is a change in intensity distribution between the signals arising from tungsten reduction: with increasing duration of calcination at 873 K, the signal of W distant from V increased at the expense of the signal indicating vicinity between W and V (Fig. 9a). After 7 days (≈10,000 min) at 873 K, the former was indeed smaller than the latter. At the same time, new intensity appeared between 900 and 1000 K, maybe shifted there from the low-temperature range, but also from the leading edge of the asymmetric 1100 K signal.

These trends seem to continue in the 1023 K calcination series. Notably, the TPR profile obtained after 5 min calcination, which was run only to 1073 K, is completely identical in the low-temperature range with that after 7 days at 873 K, which is repeated for comparison in Fig. 9b. The high-temperature signal was, however, downshifted from 1113 K to 1085 K. Already after 30 min calcination, it had turned into a small summit topping a hill with a broad maximum below 1000 K. Further calcination went on shifting low-temperature intensity to higher temperatures (2 h) and almost completely removed it (16 h). Meanwhile, the high-temperature region developed surprisingly: while two less-pronounced maxima appeared after 2 h calcination time, a pronounced peak at 1040 K showed up after 16 h (960 min), which is reminiscent of the peak caused by W(IV) → W(0) reduction in the mildly calcined samples, but has most likely a different origin. In this sample, the onset towards further reduction around 1200 K was very strong.

The development of TPR profiles during calcination at 1023 K is not well understood at present. The elucidation of their background certainly deserves attention given the high catalytic activity in the third maximum at just 20 m^2/g external surface area (Fig. 4d). Calcination at 873 K obviously results in less interaction between V and W, and therefore more formation of binary V-O-V sites. On the basis of WO_3 segregation observed by XRD and by Raman spectroscopy (Figs. 6 and 7), it appears that TPR reflects the first stages of this segregation: the detachment of surface tungstate species from the surface, without yet formation of an oxide phase. This segregation occurs in a range of calcination conditions which produces some of the activity maxima observed (cf. in particular Figs. 2, 4 a).

3.2.5. Surface analysis: XPS and low-energy ion sputtering (LEIS)

XPS of V_2O_5-WO_3/TiO_2 systems is a rather intricate task: the V 2p line is affected by X-ray satellites of the intense O 1 s line, which must be accurately corrected for, the W 4f line is superimposed by the intense Ti 3p line of the support and by the W 5p line. Representative spectra are shown in Fig. S2, together with an example for our attempts to fit the W 4f region. Apparently, W 4f is a minority component in this region, the intensity of which can be established only with considerable error. Therefore, we report here only V $2p_{3/2}$ binding energies (Table 2).

In the reference state, this binding energy was higher than known for V(V) in V_2O_5 (≈517.5 eV), after severe calcination, it was consistently below 517 eV, which suggests assignment to V(IV). However, assignment of XPS binding energies is non-trivial because structural effects may exert strong influence. In earlier work, we have observed V $2p_{3/2}$ binding energies below 517 eV for CeO_2-supported V_2O_5 [18]. Both our EPR and our TPR data (H_2 consumptions of mildly calcined samples [51]) suggest that vanadium is indeed in predominantly in the +5 state. EPR shows isolated V(IV) coexisting with V(IV) in oligomeric structures. V phases providing EPR spectra after 7d at 873 K and after 16 h at 1023 K, which exhibit dramatic differences in intensity (Fig. 8), appear at almost the same XPS binding energy (516.4 and 516.6 eV, respectively, Table 2). This shows that the differences in V(IV) concentration tracked by EPR cover only a small part of the vanadium present. Therefore, V(IV) species registered by EPR are minority sites in phases which consist predominantly of V(V), despite the low XPS binding energy. Autoreduction of V(V) during severe calcination, which has been proposed in ref. [44] and might indeed have been suspected on the basis of our EPR spectra (Fig. 8b), appears to be also a minority phenomenon in our samples, because there are no significant tendencies in the binding energy with calcination temperature.

LEIS spectra in a sequence of successive sweeps over the sample surfaces subjected to different calcination treatments are exemplified in Fig. 10. LEIS is ideally surface sensitive, but a destructive technique [63–65]. Therefore such series reflect the development of surface elemental concentrations as atomic layers are gradually sputtered away. Ti and V cannot be differentiated due to their similar atomic masses.

In Fig. 10a, it appears that the peak arising from Ti and V increases during sputtering while the tungsten peak remains constant. Closer inspection shows, however, that the latter decreases slightly, hardly beyond experimental error at these small peak sizes, and the increase of the (Ti + V) peak is smaller than suggested by optical impression due to baseline shifts as indicated in the figure. On the whole, the series is well in accordance with a model in which a monolayer of WO_x and VO_x species is sputtered from TiO_2 surfaces that are mostly not normal to the analysis direction. The tungsten peaks in Fig. 10b and c are significantly higher and the dynamics of their decrease and of the growth of the (Ti + V) signal are much stronger than in Fig. 10a. This agrees well with the expectation that WO_x species decorating the surface layer of VO_x (+WO_x) sites on TiO_2 are sputtered away first.

Intensity ratios between the (Ti + V) and W peaks in the first spectrum are given for different treatments in Table 2. Calcination at 873 K results in a strong relative increase of the W signal, i.e. in a decrease of the (Ti + V)/W ratio. After 5 min at 1023 K (2nd maximum, cf. Fig. 4d), this ratio is even smaller than after 8 h at 873 K (minimum before 2nd maximum), and it goes on decreasing towards the third maximum, which appears after 2 h at 1023 K. Notably, after 16 h at 1023 K, tungsten was less exposed than before, i.e. the (Ti + V)/W ratio increased again.

3.3. Calcination and development of SCR activity

The data presented above reveal a complicated development of surface reactivity and surface structure upon thermal treatment of V_2O_5-WO_3/TiO_2 catalysts. When starting from a mildly calcined surface providing V and W surface oxide species as arranged spontaneously during interaction with the aqueous impregnation solution, this development may proceed via three maxima of the SCR activity. The actual development depends on the relation between V and W oxide contents, initial BET surface area, and calcination rate, which is influenced by temperature and water content in the feed. With a catalyst containing 1.5 wt-% V_2O_5 and 10% WO_3 deposited on anatase of ≈140 m^2/g from the sulfate process, three activity maxima were clearly discerned at an intermediate calcination rate ($T_{calc.}$ = 973 K, cf. Fig. 4c). At higher calcination rate ($T_{calc.}$ = 1023 K, Fig. 4d), the first maximum could not be resolved, at low calcination rate ($T_{calc.}$ = 873 K, Fig. 4a), it was not well developed and therefore difficult to identify. At this calcination temperature, the third maximum could be only hypothesized because of surface changes developing on a very extended time scale.

With the sample mentioned above, peak activities after calcination were significantly larger than in the reference state obtained by fixation of the spontaneous metal oxide distribution from impregnation. However, the relation between activities in the initial state and after thermal treatments apparently also depends on the relation between V and W oxide contents and the initial

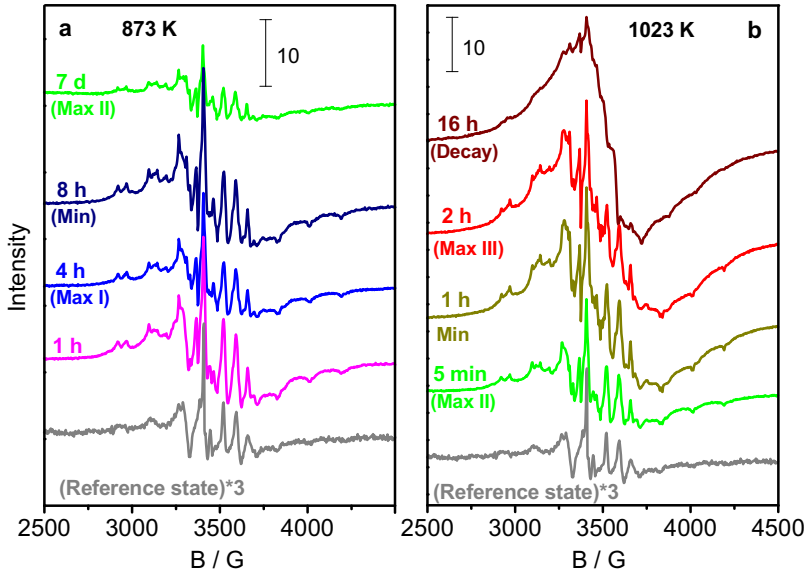

Fig. 8. EPR spectra of $V_{1.5}W_{10}$ after the reference calcination (623 K, 1 h) and after different times at 873 K (a) or 1023 K.

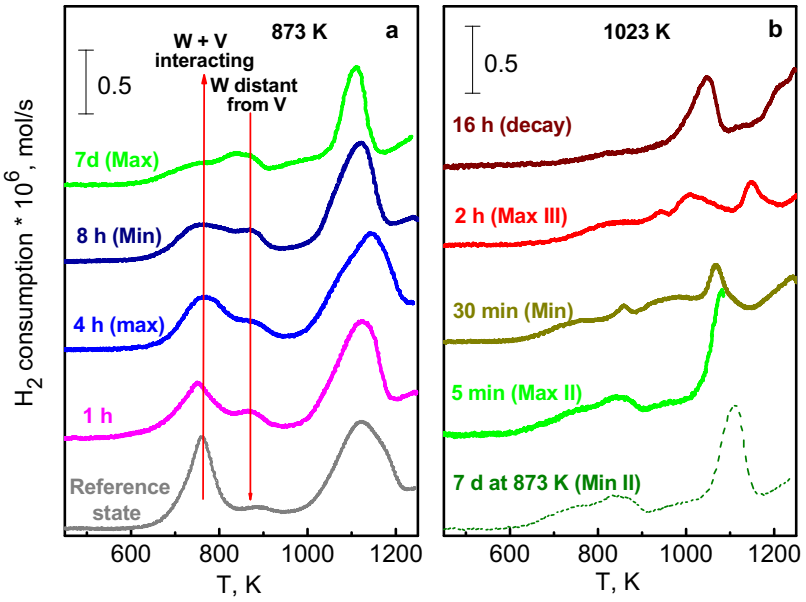

Fig. 9. TPR profiles of $V_{1.5}W_{10}$ after the reference calcination (623 K, 1 h) and after different times at 873 K (a) or 1023 K.

Table 2
Development of surface properties with increasing calcination severity: initial intensity ratios between (Ti + V) and W LEIS signals (cf. Fig. 10) and V 2p XPS binding energy.

Treatment	BET surface area, m^2/g	Approximate surface coverage[a]	(Ti + V)/W intensity ratio (LEIS)	V $2p_{3/2}$ B.E., eV
Reference calcination	142	0.8	7.6	518.2
873 K, 1 h	77	1.4	4.5	516.2
873 K, 8 h[b]	68	1.6	4.0	516.2
873 K, 168 h[c]	43	1.6	–	516.4
1023 K, 5 min	42	2.6	3.3	516.4
1023 K, 2 h	19	5.8	2.5	516.5
1023, 16 h[d]	5	22	3.2	516.6

[a] estimated total coverage, V + W.
[b] 480 min.
[c] ≈10,000 min.
[d] 960 min.

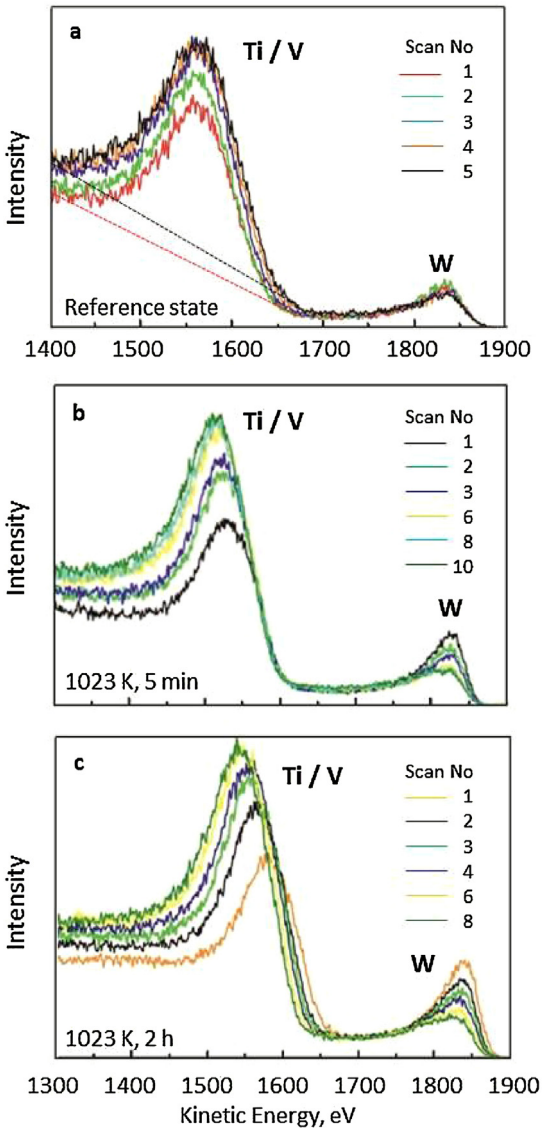

Fig. 10. LEIS spectra of $V_{1.5}W_{10}$ after the reference calcination (623 K, 1 h); a) and after different times at 1023 K – b) 5 min, c) 2 h; different scans of sputter series are reported (see label in figures).

BET surface area (Fig. 5c, d): thermal treatment may cause even exclusively damage in unfavorable cases (cf. Fig. 5d). The interplay between these parameters and the parameter range where calcination produces highly active catalysts with long lives will have to be elucidated in future studies. In industrial practice, freshly prepared catalysts are calcined under conditions identified as favorable in preceding research. On the background of the present results it is very difficult to understand which state of the catalyst is achieved by such a standard procedure and to predict trends to be expected. It is, however, very likely that a more detailed examination of the field may create the basis for such predictions and may reveal a considerable optimization potential. Nowadays, active components are often supported on titania modified with SiO_2, which delays loss of the support surface [44,45]. It might be interesting to find out if similar phenomena occur on such modified surfaces as well where silica species exert an additional separating effect.

From our characterization data, it appears that the shrinking BET surface area is the parameter by and large controlling the appearance of activity maxima and minima. On the other hand, there is no feature in the characterization results which could be directly correlated with the course of the SCR activity varying with treatment severity. We have therefore tried to combine important trends of structural features revealed in the characterization studies to a picture which might explain the activity trends on the basis of the general assumption that bridged V-O-V sites are substantially more active than isolated V oxo sites. We have chosen this approach without considering if ammonia is bound on a Brønsted or on a Lewis site in such group, but we have disregarded a decisive role of isolated vanadate species on the basis of our EPR data. The model thus derived covers the first and the second activity maximum, the third one will remain unexplained.

The basic observation from all characterization data is the preferential segregation of surface tungstate species from the support surface while evidence for segregated vanadate species or even new V-Ti-O bulk phases has not been found even after the most severe treatment. Segregation of tungsten oxide species is clearly documented by signals indicating bulk WO_3 in XRD (Fig. 6) and in Raman spectra (Fig. 7). However, the development of the ratio between TPR features assigned to W close to or far from surface vanadate (Fig. 9) and the increased abundance of W in the outmost surface layer after thermal treatments (Fig. 10, LEIS) starts well before WO_3 can be identified by XRD or even in the Raman spectra. We presume therefore that isolation of surface VO_x species by interaction with WO_x sites in the surface oxide phase formed during interaction with the impregnation liquid is excessive and unfavorable from the viewpoint of SCR activity. Removal of tungstate species from the surface therefore results in enhanced formation of more active bridged V-O-V groups, and therefore in increasing activity. Starting from the reference state of our standard catalyst (1.5 wt-% V_2O_5, 10% WO_3 on TiO_2 [ca. 140 m^2/g]), calcined at 623 K for 1 h, this activity increase is superimposed on an initially decreasing tendency (cf. Fig. 4a). As the NH_3 adsorption capacity of the bare (sulfate containing) support has been found to favor the SCR performance of V-W-TiO_2 catalysts [66] we assume that the loss of free support surface in the initial phase of the treatment may be the reason for this decay.

So far, our model covers one maximum at best: it does not explain why there is more than one activity peak and why activity decays despite ongoing segregation of tungstate. As to the problem of multiple peaks, we recall that the first activity peak is not related to a narrow range of the BET surface area and is more pronounced at higher calcination temperatures (Fig. 4). It is obviously influenced by the rate of a process, and we propose that this is the rate of water release during calcination. Obviously, the hydroxyl groups contained in the freshly prepared catalyst are removed in a shorter time during calcination at higher temperatures, which results in a high water partial pressure during the initial phase of calcination. We suppose that this moisture additionally favors the segregation of surface tungstate from the support and therefore causes enhanced SCR activity. Under such conditions, the amount of tungstate removed from the supported mixed oxide phase is apparently larger than the amount forced out just by the limit of the actual BET surface area, which would probably have been realized by a very slow calcination procedure. With ongoing calcination time, however, calcination rate and rate of water release decrease at all temperatures, and we presume that this allows some of the excessively segregated tungstate species, which are not yet stabilized by forming a new (WO_3) phase, to return to the support surface, again separating V-O-V structures. Such re-separation of V-O-V structures would explain the decreased activity after the first maximum and its almost complete absence at the lowest calcination temperature of 873 K (Fig. 4a). When proceeding towards the second maximum, the tungstate species become displaced from the surface again, but now controlled exclusively by the limitation of the available support surface, which results in very similar activities independent of the calcination temperature.

Up to now, segregation of tungstate from the mixed surface oxide phase has been considered only as a process resulting in

increased SCR activity. However, after the second maximum, where tungstate segregation apparently goes on, activity decreases significantly, most likely to an extent that could not be explained only by losses in the BET surface area. Comparison of reaction rates on a first-order basis suggests that the catalyst lost about half of its activity when proceeding from 5 min to 30 min at 1023 K (Fig. 4d) while the BET surface area decreased by ca. 40%. The discrepancy would be even larger after 15 min where activity has already fallen to the 50% level while the BET surface area (not measured) should be significantly above the 26 m^2/g obtained after 30 min. This would mean that segregation of tungstate can have also a negative effect on activity if proceeding in excess. This conclusion, which can be derived only on a tentative basis from the present data, is most convincingly supported by results published already in ref. [19]: for V_2O_5/TiO_2 catalysts with V_2O_5 contents between 0.5 and 5 wt%, activity was found to increase in all cases when adding 10% WO_3–without any adjustment of vanadate separation by thermal segregation of tungstate. In other words, this means that surface vanadates were always less active without W present, i.e. complete removal of W has a negative effect.

This raises the question if the activity of 2-dimensional oligomeric V-O-V species may decrease with increasing size of the islands, or if there is indeed a direct influence of surface tungstate species on adjacent vanadate sites, e.g. by increasing their acidity. In the first case, the only role of W would be that of a spacer controlling the arrangement of the vanadate species. In the second case, which seems counterintuitive at the first glance given the favorable effect of tungstate removal, tungsten would influence the system in different modes: if in excess, it would interfere with the formation of the more active V-O-V sites, if in proper concentration, it would enhance their activity. On the basis of the present data, these options cannot be differentiated. As it seems unlikely that the size of surface vanadate islands can be controlled without a spacer component, the most promising approach towards a decision of this question may be a study with a vanadium-rich system promoted by very small amounts of tungstate. This may give the chance to separate the direct influence of tungstate on vanadate from its spacer effect which should be insignificant in presence of large vanadate excess.

As mentioned above, the model presented has been designed to explain the fluctuation of SCR activity with increasing severity of the treatment in a rational way, taking into account as much of the characterization data as possible. A feature neglected in this discussion is that segregated tungstate species may cover part of the surface mixed oxide phase (cf. LEIS data, Section 3.2.5) and might thus adversely affect also active V-O-V sites. It is, however, difficult to assess the extent of this effect, which will be counteracted by the formation of the WO_3 phase under more severe conditions. The TPR data (Section 3.2.4., intensity shift from signal of W interacting with V towards signal of W distant from V) might suggest that much of the segregated W interacts with tungstate species still anchored to the surface.

The most serious shortcoming of our model is, of course, its inability to explain the third, very pronounced activity maximum, which appears at ca. 20 m^2/g with $V_{1.5}W_{10}$. Obviously, severe thermal treatment does not just invert the insertion of the tungstate species between the surface vanadate entities, but it may apparently result also in solid-state reactions producing a new as yet unidentified phase or surface state possibly comprising all three transition metals present. The unidentified phase is amorphous. We did not find any promising hint on the nature of this phase or state in our characterization data obtained from the sample at the third maximum, which are anyway difficult to interpret due to the inclusion of a significant part of the external surface inside polycrystalline aggregates. The high activity exhibited at a rather low BET surface area (even at 5 m^2/g, peak conversion was still 55% at 750,000 h^{-1}, cf. Fig. 4d) makes the identification of this phase or surface state an interesting goal for future studies.

4. Conclusions

When subjected to thermal stress in dry or moist air, V_2O_5-WO_3/TiO_2 catalysts initially calcined under mild conditions exhibit a complex behavior driven by the progressive loss of support surface area. Depending on the calcination temperature, up to three maxima of the SCR activity may be observed before the latter dies off. While the first of these maxima depends on the calcination rate (temperature) and may be missed at a low rate, the other two maxima occur at specific ranges of the BET surface area. With a catalyst containing 1.5 wt-% V_2O_5 and 10 wt-% WO_3 on anatase of initially 140 m^2/g, these ranges were ≈42 m^2/g and ≈20 m^2/g, respectively. Structural characterization of the sample in different states revealed that loss of support surface area results in segregation of exclusively tungstate species from the support surface. These aggregate to WO_3 detectable by Raman spectroscopy and XRD while no evidence was found for the formation of vanadium-containing compounds even under the most severe conditions. Observations in the EPR spectra contradict correlation of SCR activities with the abundance of isolated vanadate sites. Assuming major contributions of bridged vanadate sites to the catalytic performance, a model was proposed that allows explaining the first two activity maxima though failing with the third one. In this model, segregation of tungstate results in formation of highly active V-O-V structures from less active isolated vanadate species previously separated by excessive amounts of tungstate. In this notion, the role of tungstate is to provide optimum sizes of vanadate ensembles. An experimental strategy is proposed which will allow deciding if there is an additional favorable tungstate influence on the vanadate sites or if the activity loss after the second maximum results from decreasing intrinsic activity of larger vanadate islands.

Ackowledgements

We acknowledge gratefully experimental support by Dr. Elke Löffler, Ruhr University Bochum (“RUB”; FT Raman spectroscopy), Dr. T. Reinecke, RUB (XRD), Dr. Inga Ellmers, RUB (XPS, LEIS), Ms. Susanne Buse, RUB (BET, TPR) and by Dipl.-Ing. M. Kappa, Brandenburg Technical University Cottbus (XRD).

Appendix A. Supplementary data

Supplementary data associated with this article can be found, in the online version, at http://dx.doi.org/10.1016/j.apcatb.2017.06.006

References

[1] H. Bosch, F.J.J.G. Janssen, Catal. Today 2 (1988) 369–531.
[2] Urea-SCR Technology for deNOx After Treatment of Diesel Exhausts, in: I. Nova, E. Tronconi (Eds.), Springer, Berlin-Heidelberg-New York, 2014.
[3] L. Lietti, P. Forzatti, F. Bregani, Ind. Eng. Chem. 35 (1996) 3884–3892.
[4] G. Madia, M. Elsener, M. Koebel, F. Raimondi, A. Wokaun, Appl. Catal. B 39 (2002) 181–190.
[5] W. Weisweiler, Chem. Ing. Techn. 72 (2000) 441–449.
[6] L.J. Alemany, L. Lietti, N. Ferlazzo, P. Forzatti, G. Busca, E. Giamello, F. Bregani, J. Catal. 155 (1995) 117–130.
[7] J.P. Chen, R.T. Yang, Appl. Catal. A 80 (1992) 135–148.
[8] G. Ramis, G. Busca, C. Cristiani, L. Lietti, P. Forzatti, F. Bregani, Langmuir 119 (1992) 1744–1749.
[9] I.E. Wachs, J. Catal. 124 (1990) 570–573.
[10] G.T. Went, S.T. Oyama, A.T. Bell, J. Phys. Chem. 94 (1990) 4240–4246.
[11] I.E. Wachs, Catal. Today 100 (2005) 79–94.
[12] M.A. Vuurman, I.E. Wachs, A.M. Hirt, J. Phys. Chem. 95 (1991) 9928–9937.
[13] H. Eckert, I.E. Wachs, J. Phys. Chem. 93 (1989) 6796–6805.
[14] G.T. Went, L.J. Leu, A.T. Bell, J. Catal. 134 (1992) 479–491.
[15] G.C. Bond, Appl. Catal. A 157 (1997) 91–103.

[16] H.J. Tian, E.I. Ross, I.E. Wachs, J. Phys. Chem. B 110 (2006) 9593–9600.
[17] M.A. Banares, I.E. Wachs, J. Raman Spectrosc. 33 (2002) 359–380.
[18] L.E. Briand, O.P. Tkachenko, M. Guraya, X. Gao, I.E. Wachs, W. Grünert, J. Phys. Chem. B 108 (2004) 4823–4830.
[19] P.G.W.A. Kompio, A. Brückner, F. Hipler, G. Auer, E. Löffler, W. Grünert, J. Catal. 286 (2012) 237–247.
[20] L. Lietti, P. Forzatti, Appl. Catal. B 3 (1993) 13–35.
[21] F.J.J.G. Janssen, F. van den Kerkhof, H. Bosch, J. Ross, J. Phys. Chem. 91 (1987) 5921–5927.
[22] F.J.J.G. Janssen, F. van den Kerkhof, H. Bosch, J. Ross, J. Phys. Chem. 91 (1987) 6633–6638.
[23] G.T. Went, L.J. Leu, R.R. Rosin, A.T. Bell, J. Catal. 134 (1992) 492–505.
[24] M.D. Amiridis, I.E. Wachs, G. Deo, J.-M. Jehng, D.J. Kim, J. Catal. 161 (1996) 247–253.
[25] I.E. Wachs, G. Deo, B.M. Weckhuysen, A. Andreini, M.A. Vuurman, M. de Boer, M.D. Amiridis, J. Catal. 161 (1996) 211–221.
[26] M. Inomata, A. Miyamoto, Y. Murakami, J. Catal. 62 (1980) 140–148.
[27] M. Wark, A. Brückner, T. Liese, W. Grünert, J. Catal. 175 (1998) 48–61.
[28] G. Piehl, T. Liese, W. Grünert, Catal. Today 54 (1999) 401–406.
[29] G. Ramis, G. Busca, F. Bregani, P. Forzatti, Appl. Catal. 64 (1990) 2259–2278.
[30] L. Lietti, G. Ramis, F. Berti, G. Toledo, D. Robba, G. Busca, P. Forzatti, Catal. Today 42 (1998) 101–116.
[31] U.S. Ozkan, Y.P. Cai, M.W. Kumthekar, J. Catal. 149 (1994) 390–403.
[32] M. Gasior, J. Haber, T. Machej, T. Czeppe, J. Mol. Catal. 43 (1988) 359–369.
[33] N.-Y. Topsoe, H. Topsoe, Catal. Today 9 (1991) 77–82.
[34] N.-Y. Topsoe, J.A. Dumesic, H. Topsoe, J. Catal. 151 (1995) 241–252.
[35] N.-Y. Topsoe, H. Topsoe, J.A. Dumesic, J. Catal. 151 (1995) 226–240.
[36] N.-Y. Topsoe, Science 265 (1994) 1217–1219.
[37] J.A. Dumesic, N.-Y. Topsoe, H. Topsoe, Y. Chen, T. Slabiak, J. Catal. 163 (1996) 409–417.
[38] A. Marberger, D. Ferri, M. Elsener, O. Kröcher, Angew. Chem. Intern. Ed. 55 (2016) 11989–11994.
[39] E. Broclawik, A. Gora, M. Najbar, J. Mol. Catal. A 166 (2001) 31–38.
[40] J.W. Choung, I.S. Nam, S.W. Ham, Catal. Today 111 (2006) 242–247.
[41] G. Oliveri, G. Ramis, G. Busca, V.S. Escribano, J. Mat. Chem. 3 (1993) 1239–1249.
[42] C. Cristiani, M. Belotto, P. Forzatti, F. Bregani, J. Mater. Res. 8 (1993) 2019–2025.
[43] I. Nova, L. dall'Acqua, L. Lietti, E. Giamello, P. Forzatti, Appl. Catal. B 35 (2001) 31–42.
[44] A.M. Beale, I. Lezcano-Gonzalez, T. Maunula, R.G. Palgrave, Catal. Struct. React. 1 (2015) 25–34.
[45] S. Augustine, J. Schultz, R. McIntyre, Catal. Today 112 (2006) 180–183.
[46] M. Kobayashi, M. Hagi, Appl. Catal. B 62 (2006) 104–113.
[47] Product Information, Huntsman P&A Germany, 2016.
[48] J.P. Dunn, H.G. Stenger Jr., I.E. Wachs, J. Catal. 181 (1999) 233–243.
[49] K. Bourikas, C. Fountzoula, C. Kordulis, App. Catal. B 52 (2004) 145–153.
[50] P.G.W.A. Kompio, W. Grünert, F. Hipler, unpublished results.
[51] P.G.W.A. Kompio, PhD Thesis, Bochum, 2010.
[52] G. Centi, Appl. Catal. A 147 (1996) 267–298.
[53] T. Ohsaka, F. Izumi, Y. Fujiki, J. Raman Spectrosc. 7 (1978) 321–324.
[54] U. Balachandran, N.G. Eror, J. Solid State Chem. 42 (1982) 276–282.
[55] H. Jeziorowski, H. Knözinger, J. Phys. Chem. 83 (1979) 1166–1173.
[56] I.E. Wachs, C.A. Roberts, Chem. Soc. Rev. 39 (2010) 5002–5017.
[57] M. Reiche, T. Bürgi, A. Baiker, A. Scholz, B. Schnyder, A. Wokaun, Appl. Catal. A 198 (2000) 155–169.
[58] C. Wang, S. Yang, H. Chang, Y. Peng, J. Li, Chem. Eng. J. 225 (2013) 520–527.
[59] S.B. Xie, E. Iglesia, A.T. Bell, Langmuir 16 (2000) 7162–7167.
[60] S.S. Chan, I.E. Wachs, L.L. Murrell, J. Catal. 90 (1984) 150–155.
[61] J.P. Baltrus, L.E. Makovsky, J.M. Stencel, D.M. Hercules, Analyt. Chem. 57 (1985) 2500–2503.
[62] M. Li, Z. Feng, G. Xiong, P. Ying, Q. Xin, C. Li, J. Phys. Chem. B 105 (2001) 8107–8111.
[63] H.R.J. ter Veen, T. Kim, I.E. Wachs, H.H. Brongersma, Catal. Today 140 (2009) 197–201.
[64] H.H. Brongersma, M. Draxler, M. de Ridder, P. Bauer, Surf. Sci. Rep. 62 (2007) 63–109.
[65] N. Kruse, S. Chenakin, Characterisation of Solid Materials: From Structure to Surface Reactivity, in: M. Che, J.C. Vedrine (Eds.), Wiley-VCH Weinheim, 2012, pp. 453–510.
[66] C. Orsenigo, L. Lietti, E. Tronconi, P. Forzatti, F. Bregani, Ind. Eng. Chem. Res. 37 (1998) 2350–2359.